Research Article | Vol. 24, No. 22 | 31 Oct 2016 | OPTICS EXPRESS 25211

Optics EXPRESS

Distributed shape sensing using Brillouin scattering in multi-core fibers

ZHIYONG ZHAO,[1,2] MARCELO A. SOTO,[1] MING TANG,[2,3] AND LUC THÉVENAZ[1,4]

[1]*EPFL, Swiss Federal Institute of Technology, Institute of Electrical Engineering, SCI-STI-LT Station 11, CH-1015 Lausanne, Switzerland*
[2]*Wuhan National Lab for Optoelectronics (WNLO) & National Engineering Laboratory for Next Generation Internet Access System, School of Optics and Electronic Information, Huazhong University of Science and Technology, Wuhan 430074, China*
[3]*tangming@mail.hust.edu.cn*
[4]*luc.thevenaz@epfl.ch*

Abstract: A theoretical and experimental study on the response of Brillouin scattering in multi-core optical fibers (MCF) under different curving conditions is presented. Results demonstrate that the Brillouin frequency shift of the off-center cores in MCF is highly bending-dependent, showing a linear dependence on the fiber curvature. This feature is here exploited to develop a new kind of distributed optical fiber sensor, which provides measurements of a distributed profile mapping the longitudinal fiber shape. Using conventional Brillouin optical time-domain analysis with differential pulse-width pairs, fully distributed shape sensing along a 1 km-long MCF is practically demonstrated. Experimental results show a very good agreement with the theoretically expected behavior deduced from the dependence of the Brillouin frequency on the strain induced by the fiber bending over a given core. The analysis and results presented in this paper constitute the first demonstration of distributed bending sensing, providing the cornerstone to further develop it into a fully distributed three-dimensional shape sensor.

OCIS codes: (060.2310) Fiber optics; (060.2370) Fiber optics sensors; (290.5900) Scattering, stimulated Brillouin.

References and links

1. A. Motil, A. Bergman, and M. Tur, "State of the art of Brillouin fiber-optic distributed sensing," Opt. Laser Technol. **78**, 81–103 (2016).
2. M. A. Soto and L. Thévenaz, "Modeling and evaluating the performance of Brillouin distributed optical fiber sensors," Opt. Express **21**(25), 31347–31366 (2013).
3. X. Bao and L. Chen, "Recent progress in Brillouin scattering based fiber sensors," Sensors (Basel) **11**(4), 4152–4187 (2011).
4. L. Thévenaz, "Brillouin distributed time-domain sensing in optical fibers: state of the art and perspectives," Front. Optoelectron. China **3**(1), 13–21 (2010).
5. M. Niklès, L. Thévenaz, and P. A. Robert, "Brillouin gain spectrum characterization in single-mode optical fibers," J. Lightwave Technol. **15**(10), 1842–1851 (1997).
6. L. Zou, X. Bao, S. Afshar V, and L. Chen, "Dependence of the brillouin frequency shift on strain and temperature in a photonic crystal fiber," Opt. Lett. **29**(13), 1485–1487 (2004).
7. Y. Mizuno and K. Nakamura, "Potential of Brillouin scattering in polymer optical fiber for strain-insensitive high-accuracy temperature sensing," Opt. Lett. **35**(23), 3985–3987 (2010).
8. K.-Y. Song and Y.-H. Kim, "Characterization of stimulated Brillouin scattering in a few-mode fiber," Opt. Lett. **38**(22), 4841–4844 (2013).
9. J.-C. Beugnot, S. Lebrun, G. Pauliat, H. Maillotte, V. Laude, and T. Sylvestre, "Brillouin light scattering from surface acoustic waves in a subwavelength-diameter optical fibre," Nat. Commun. **5**, 5242 (2014).
10. B. Li, Z. Feng, M. Tang, Z. Xu, S. Fu, Q. Wu, L. Deng, W. Tong, S. Liu, and P. P. Shum, "Experimental demonstration of large capacity WSDM optical access network with multicore fibers and advanced modulation formats," Opt. Express **23**(9), 10997–11006 (2015).
11. L. Yuan, J. Yang, Z. Liu, and J. Sun, "In-fiber integrated Michelson interferometer," Opt. Lett. **31**(18), 2692–2694 (2006).
12. G. M. H. Flockhart, W. N. MacPherson, J. S. Barton, J. D. C. Jones, L. Zhang, and I. Bennion, "Two-axis bend measurement with Bragg gratings in multicore optical fiber," Opt. Lett. **28**(6), 387–389 (2003).

#274737 http://dx.doi.org/10.1364/OE.24.025211
Journal © 2016 Received 31 Aug 2016; revised 16 Oct 2016; accepted 17 Oct 2016; published 19 Oct 2016

Optics EXPRESS

13. L. Yuan, J. Yang, and Z. Liu, "A compact fiber-optic flow velocity sensor based on a twin-core fiber Michelson interferometer," IEEE Sens. J. **8**(7), 1114–1117 (2008).
14. A. Fender, W. N. MacPherson, R. R. J. Maier, J. S. Barton, D. S. George, R. I. Howden, G. W. Smith, B. J. S. Jones, S. McCulloch, X. F. Chen, R. Suo, L. Zhang, and I. Bennion, "Two-axis temperature-insensitive accelerometer based on multicore fiber Bragg gratings," IEEE Sens. J. **8**(7), 1292–1298 (2008).
15. J. P. Moore and M. D. Rogge, "Shape sensing using multi-core fiber optic cable and parametric curve solutions," Opt. Express **20**(3), 2967–2973 (2012).
16. Y. Mizuno, N. Hayashi, H. Tanaka, Y. Wada, and K. Nakamura, "Brillouin scattering in multi-core optical fibers for sensing applications," Sci. Rep. **5**, 11388 (2015).
17. W. Li, X. Bao, Y. Li, and L. Chen, "Differential pulse-width pair BOTDA for high spatial resolution sensing," Opt. Express **16**(26), 21616–21625 (2008).

1. Introduction

Over the past 30 years the optical fiber sensing technology has undergone a tremendous development, in which Brillouin distributed optical fiber sensing has decisively contributed thanks to its key advantages to perform distributed measurements along very long distance [1,2]. The high performance achieved by Brillouin distributed sensing has made this technique one of the most remarkable and promising fiber optic sensing technologies existing nowadays [1–4]. Brillouin distributed fiber sensors have so far been mostly dedicated to measure distributed strain and temperature profiles [1–5] along conventional single-mode optical fibers, being recently extended to photonic crystal fiber [6], polymer optical fiber [7], few mode fiber [8], and micro-/nano-fiber [9], among others.

On the other hand, multi-core fibers (MCF) have been developed in recent years to cope with the exponential growth of internet traffic and the associated ever increasing demand [10]. Using schemes based on space division multiplexing (SDM) in MCF a significant increase in transmission capacity has been successfully demonstrated, rising a considerable worldwide interest for MCFs [10]. The features of MCFs, consisting in fibers with a transversal structure containing more than one core within a single cladding, have also found applications in the field of optical fiber sensing. Multi-core fiber based sensors have been used for bending and curvature sensing [11,12], or for indirectly measuring quantities inducing a cantilever bending, such as flow velocity sensors [13] and accelerometers [14]. Ultimately their potentiality for shape sensing has been pointed out and demonstrated [15]. All these reported transducers are however fiber-based point (discrete) sensors, which do not exploit the distributed sensing capabilities offered by the optical fiber. MCFs have been only recently investigated for distributed strain and temperature sensing based on stimulated Brillouin scattering [16]. Reference 16 actually reports that temperature and strain sensitivities of Brillouin scattering in any core of a MCF are comparable and essentially identical to standard single-core optical fibers. However, the particular feature of having multiple cores inside a MCF has not been fully explored so far for novel sensing applications, such as retrieving a distributed profile containing transversal spatial information in a MCF. More specifically, the potential of the differential response between the cores has not yet been crucially addressed for distributed sensing.

In this paper the spectral response of Brillouin scattering is investigated for bending and curvature sensing. In particular, the dependence of the Brillouin frequency shift (BFS) of off-center cores on the geometric fiber parameters is theoretically described; this includes the dependence on the relative orientation between cores and the bending direction, on the curvature (the reciprocal of bending radius), and on the distance between the outer and central cores in the MCF. Theoretical and experimental results demonstrate that the Brillouin frequency of outer cores is highly sensitive to bending due to the local tangential strain induced at the bending point. In particular, a linear dependence of BFS on the fiber curvature is experimentally and theoretically verified in a 7 core MCF. After fiber characterization, distributed shape sensing using the differential response between cores is experimentally demonstrated, for the first time to the best of our knowledge, along a 1 km-long MCF. Results convincingly support the perspective that standard Brillouin sensing methods can be exploited

Optics EXPRESS

to measure curvature, thus potentially enabling fully distributed three-dimensional (3D) shape sensing.

2. Determining the bending angle and curvature based on BFS measurements in a MCF

Brillouin scattering is among the most prevalent nonlinear effects existing in optical fibers. This is generated by a strictly phase-matched coupling between optical and acoustic waves in the fiber [1]. The acoustic wave actually modulates the refractive index of the fiber, generating a grating that moves at the acoustic velocity along the fiber, and reflects a fraction of the pump signal subject to a Doppler spectral shift. This spectral shift is designated as the ν_B [1]:

$$\nu_B = \frac{2n_{eff} \cdot V_a}{\lambda} \tag{1}$$

where n_{eff} is the effective refractive index of the guided mode along the fiber, V_a is the acoustic velocity and λ is the vacuum wavelength of the pump light.

The principle of Brillouin distributed fiber sensing is based on the significant dependence of the acoustic velocity on temperature and strain. This way, by measuring the longitudinal Brillouin frequency shift (BFS) profile along an optical fiber, information about the strain and temperature distribution along this fiber can be obtained [1–5]. Fiber interrogation methods can be implemented in the time-, frequency-, or correlation-domain, depending on the target sensing conditions (e.g. spatial resolution and distance range) [1].

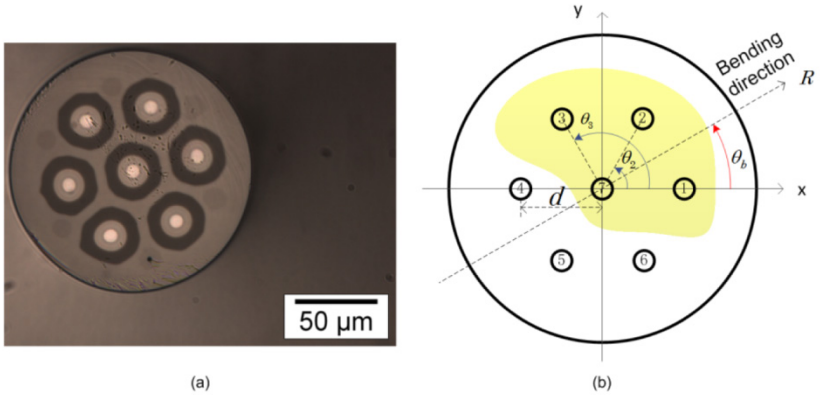

Fig. 1. (a) Cross sectional view of the 7-core fiber used in our experiment and (b) transversal distribution of the cores with the definition of the important geometrical parameters.

In this section the dependence of the BFS on longitudinal strain is investigated as a mechanism to perform distributed curvature sensing using a multi-core optical fiber. In order to provide a theoretical description of the principle here exploited, the impact of bending on the BFS of outer cores in a MCF is analyzed based on the transversal geometrical features of the fiber. For this study a 7-core MCF is used, with a central core and 6 outer cores arranged in a hexagonal array, as shown in Fig. 1(a). This figure actually shows the cross sectional view of the fiber used later for the experimental validation, which has a nominal cladding diameter of 150 μm and a core pitch *d* of 40 μm. It is worth mentioning that although this 7-core MCF is here used to illustrate and describe the proposed working principle, the analysis described hereafter is also valid for MCF with any number of cores. More specifically, in order to reliably deduce the bending direction and curvature in a 3D space, a measurement with a minimum number of three cores is required [15]. However, the use of a larger number

Optics EXPRESS

of cores provides redundancy that helps in reducing the measurement uncertainty, as explained hereafter.

Figure 1(b) illustrates the layout of the 7 cores. If the fiber is bent in a given direction, different levels of strain are induced in each fiber core. While some of the cores are expected to be affected by local compressional strain, others are expected to be locally elongated; this depends on the relative angular position between a given core and the local bending axis. In particular, the bending-induced strain in a core i, at any point along the MCF, can be described as:

$$\varepsilon_i = -\frac{d_i}{R}\cos(\theta_b - \theta_i) \tag{2}$$

where ε_i is the locally-induced strain in core i, d_i is the distance between core i and the center of the fiber, R is the bending radius, θ_b and θ_i are respectively the angle of the bending direction and the angular position of core i. In particular, θ_b is defined to be the angular offset from the local x-axis (arbitrarily chosen as reference) to the local fiber bending direction originating from the center of the curvature circle, and θ_i is the angle from local x-axis to core i, as shown in Fig. 1(b). This induced strain ε_i actually has an impact on the BFS of that given core i, shifting the Brillouin frequency in a linear proportion to the bending-induced inner strain, as:

$$\frac{\Delta\nu_{Bi}}{\nu_B} = \alpha\cdot\varepsilon_i = -\frac{\alpha\cdot d_i}{R}\cos(\theta_b - \theta_i) \tag{3}$$

where $\Delta\nu_{Bi}$ is the BFS variation of core i, α is the strain sensitivity of the relative BFS variation, ν_B is the initial BFS in a reference condition (i.e. at the present ambient temperature and without strain). It is worth mentioning that the central core is, in general, expected not to be affected by bending-induced strain, since its transversal position is always located on the strain neutral line. This is an interesting feature since the central core can be used to obtain a reference profile to compensate for the global fiber temperature changes.

In order to calculate the curvature κ of the fiber (where $\kappa = 1/R$), the principle of the here proposed method consists in measuring the BFS profile of each core along the fiber. Note that at the bending location, the BFS of each core provides redundant information about the strain induced in the fiber. Although solving Eq. (3) for a couple of cores is mathematically sufficient to retrieve the bending angle and radius, the use of the redundancy in information obtained from all cores can be used to reduce the error in the calculation [15] and to improve the reliability of the measurement. Following the model presented in [15] and summarized here for the sake of clarity, an apparent curvature vector $K_{\hat{i}}$ can be defined for each core i. The magnitude of this vector depends on the induced strain and the radial distance between the core and the fiber center, while its direction depends on the angular offset of the core [15]. Using N cores, the vector sum K of the apparent curvature vectors $K_{\hat{i}}$ is defined as [15]:

$$K(z) = -\sum_{i=1}^{N}\frac{\varepsilon_i(z)}{d_i}\cos\theta_i\hat{i} - \sum_{i=1}^{N}\frac{\varepsilon_i(z)}{d_i}\sin\theta_i\hat{j} \tag{4}$$

where $\hat{i}$ and $\hat{j}$ are unit vectors aligned with the local x- and y-axis, respectively. From Eq. (4) the local bending angle $\theta_b(z)$ and curvature $\kappa(z)$ can be calculated as:

Optics EXPRESS

$$\theta_b(z) = \cos^{-1}\left(\frac{K_{\hat{i}}(z)}{|K(z)|}\right) = \sin^{-1}\left(\frac{K_{\hat{j}}(z)}{|K(z)|}\right) = \tan^{-1}\left(\frac{K_{\hat{j}}(z)}{K_{\hat{i}}(z)}\right) \tag{5}$$

$$\kappa(z) = \frac{|K(z)|}{\sqrt{\left(\sum_{i=1}^{N}\cos(\theta_b-\theta_i)\cos(\theta_i)\right)^2+\left(\sum_{i=1}^{N}\cos(\theta_b-\theta_i)\sin(\theta_i)\right)^2}} \tag{6}$$

For the particular case of a symmetrical core distribution, e.g. symmetrically arranged tri-core fiber, in which cores are equally separated by a 2π/3 angular offset at the same radial distance from the fiber center, Eq. (6) can be simplified as:

$$\kappa(z) = \frac{2|K(z)|}{N} \tag{7}$$

3. Experimental setup

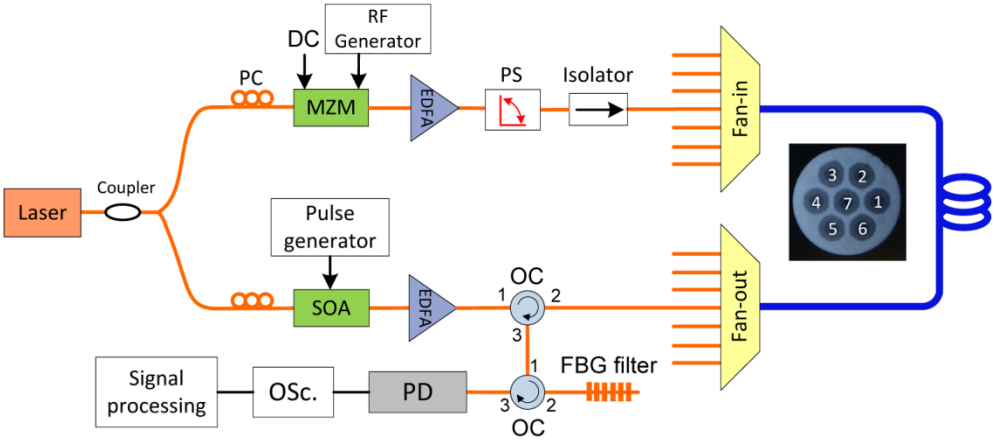

Fig. 2. Experimental setup. PC: polarization controller; MZM: Mach-Zehnder modulator; SOA: semiconductor optical amplifier; EDFA: erbium-doped fiber amplifier; PS: polarization switch; OC: optical circulator; FBG: fiber Bragg grating; PD: photodetector. OSc.: oscilloscope.

The experimental setup depicted in Fig. 2 is used to characterize the Brillouin frequency of off-center cores in a MCF, and to determine its dependence on the local bending (amount of curvature and bending direction angle). In order to obtain a sharp spatial resolution, and thus to have a more reliable characterization of the curvature due to short bending, a Brillouin optical time-domain analyzer (BOTDA) using differential pulse-width pairs (DPP) [17] has been implemented with a spatial resolution of 20 cm. For this, a standard distributed feedback (DFB) laser operating at 1551 nm is used as an optical source. The laser light is split into distinct branches. On the one hand, the upper branch in the figure is used to synthesize a two-sideband carrier-suppressed probe signal [5], which is generated by a Mach-Zehnder modulator (MZM) driven by a tunable radio frequency (RF) generator to scan the Brillouin gain spectrum (BGS) of the fiber. The probe power is boosted by an erbium-doped fiber amplifier (EDFA) to compensate for the high insertion loss of the coupling into the MCF. A polarization switch is used to mitigate the polarization-induced fading in the measured Brillouin traces by summing 2 successive measurements using orthogonal probe polarizations. On the other hand, the lower branch in Fig. 2 is used to generate the pump signal. A semiconductor optical amplifier (SOA) is employed to generate optical pulses with high extinction ratio (> 50 dB), and then another EDFA is used to get a high peak pump

Optics EXPRESS

power. The amplified pump light is connected with the pigtail of the fan-out coupler through a three-port optical circulator (OC). Square pulses with 60 ns and 58 ns durations are set for the measurements, resulting in an equivalent differential pulse of 2 ns corresponding to a 20 cm spatial resolution.

In the receiver side, the backscattered light is coupled through another three-port optical circulator to a fiber Bragg grating (FBG) in reflection mode (bandpass), which is used to filter out one of the sidebands before photo-detection and to eliminate all spurious spectral components (Rayleigh and reflections from pump, amplified spontaneous emission from EDFA). A photo-receiver of 1 GHz band and a fast oscilloscope controlled by a computer are used to acquire the time-domain BOTDA traces. Pump and probe are launched into a 1 km-long 7-core MCF. The MCF is spliced to fan-in/out spatial Mux/De-Mux couplers at each end, providing a total flexibility to assemble different configurations. After measuring the BOTDA response from a given fiber core, the process is consecutively repeated in the other cores.

4. Experimental results

4.1. BFS fluctuations in a coiled MCF

To evidence the reality of the sensitivity to curvature, a first simple test has been carried out by measuring the BGS of an off-center core along the ~1 km-long coiled MCF. In order to have a reference uniform BFS profile, the last ~31 m of fiber have been placed loosely in a straight configuration, so that no strain affects the measurement. Figure 3(a) shows the BGS distribution over the last ~100 m of fiber measured in an outer fiber core, where the first ~90 m shown in the figure correspond to the randomly oriented coiled segment in the spooling (with a diameter of ~15 cm). The measurement confirms that the BFS along the straight fiber segment spanning over the last 10 meters is uniform, while the BFS of the fiber section coiled in the spool shows random fluctuations. Those BFS fluctuations are actually induced by bending, and result from the local tangential strain induced by the fiber coiling with random orientation. In particular, based on the conventional behavior of the Brillouin frequency, the BFS is expected to be down-shifted when the off-center core is compressed and up-shifted when being stretched.

Optics EXPRESS

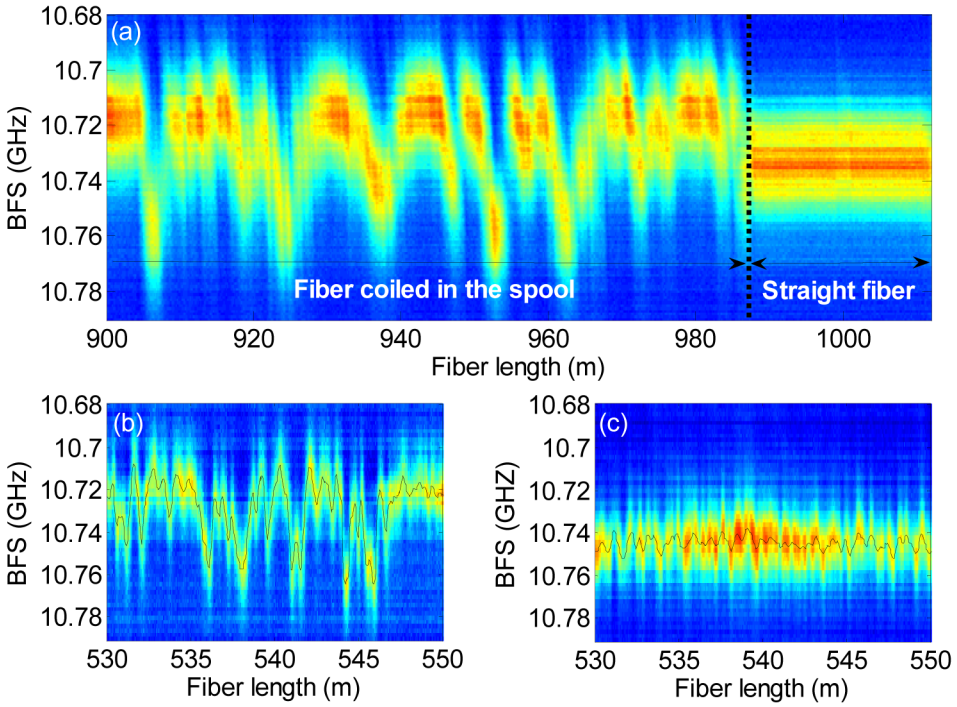

Fig. 3. Brillouin gain spectrum versus distance (a) measured along an off-center core of a MCF showing a coiled and a straight fiber regions. A zoom-in along 20 m of the coiled fiber section shows (b) BFS fluctuations measured along an off-center core and (c) a uniform BFS profile obtained along the central core.

Figure 3(b) shows a more detailed view of the BFS distribution along a 20 m fiber segment. It is important to mention that similar BFS oscillations have been observed in all outer cores of the MCF, however, a much more uniform BFS profile (similar to any normal single mode fiber) could be observed in the central core, as shown in Fig. 3(c). This provides a first evidence of the high sensitivity that the BFS of multi-core fibers exhibits to bending.

4.2. Characterization of the BFS dependence on curvature

In order to quantify the BFS dependence on the fiber curvature, a short section (~1.5 m) of the MCF (at ~997 m distance) has been bent in a precisely oriented direction when compared to the orientation of the cores in the fiber. In particular, Core 1 (see Fig. 1(b)) has been chosen to characterize the response to bending, while the bending direction has been precisely controlled to be accurately aligned along the local *x*-axis of the fiber. To reach a perfect alignment, red light has been launched into Core 1, while a microscope has been used to visualize the real positioning of the core, so that it securely lays in the applied bending plane. In the process, the two fiber ends have been tightly fixed onto two movable metal plates, which are then used to create a circle type bending without inducing any twist along the 1.5 m long fiber, with a circular bending diameter that has been adjusted for different measurements. By controlling the bending direction in a 2D plane, a bend with known characteristics (orientation and curvature) could be applied while keeping the spatial distributions of cores without twisting. This way, the angular direction of Core 1 (used as a reference axis) turns out to be equal to $\theta_1 = 0$. Furthermore, by securing the bending direction to be aligned with the defined *x*-axis, the bending direction angle θ_b is forced to be close to zero. It is actually important to mention that although the calibration of the bending angle and core positions might not be perfectly accurate, Core 1 actually exhibits the lowest sensitivity

Optics EXPRESS

to any bending plane mismatching, because the slope of the cosine function in Eq. (2) is zero at the maximum/minimum points. This feature favors a better reliability to the characterization of the impact of bending on the BFS measurements.

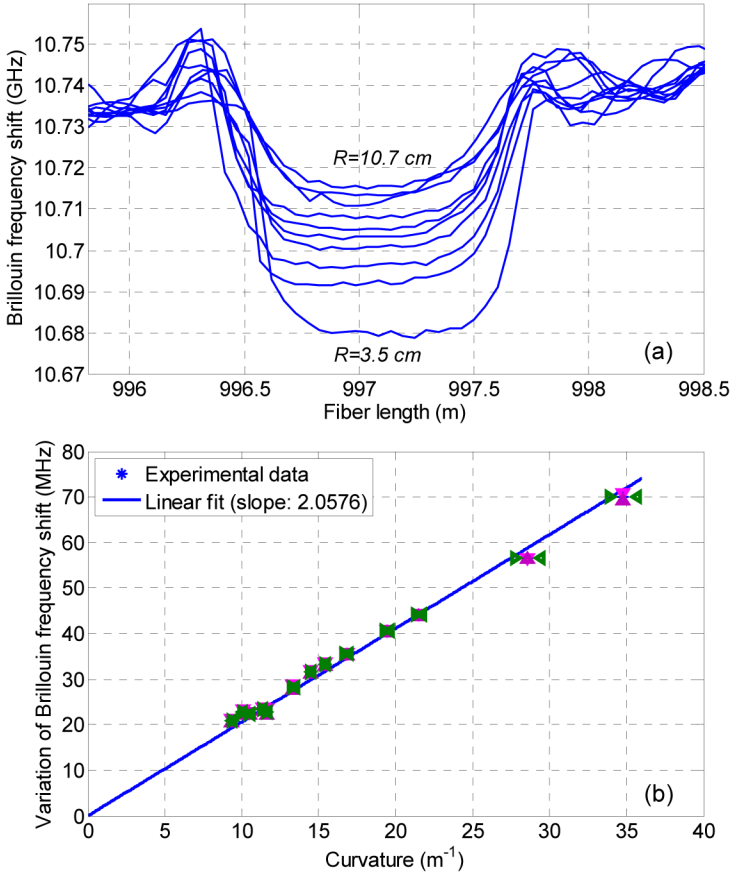

Fig. 4. (a) Extracted Brillouin frequency shift for different bending radii. (b) Dependence of BFS on curvature measured along an outer core of the MCF. The error intervals on the curvature and the measured BFS are marked in green and purple triangle dots, respectively.

Circular bending in a fiber section of about 1.5 m-long has been applied by coiling the fiber in several loops with different radii, while the BFS of Core 1 has been measured, as shown in Fig. 4(a). The figure clearly highlights the high dependence of the measured BFS on the applied curvature. At each applied curvature, the BFS measurement has been repeated 5 times to secure a better determination of the real (mean) BFS value and to quantify the uncertainty (standard deviation) on the measurements. As a reference, the BFS of the fiber without applied strain is measured to be 10.735 GHz with a frequency uncertainty of 0.8 MHz (evaluated as the standard deviation of consecutive measurements [2]). Figure 4(b) shows the measured BFS variations as a function of the applied bending curvature ($\kappa = 1/R$), demonstrating that the measurements match very well the expected linear behavior as described by Eq. (3), with a slope equal to S = 2.06 MHz/m^{-1} (obtained from a linear fitting of the data). Note that the figure also includes the uncertainty in the BFS determination (purple vertical markers), calculated as the standard deviation on 5 BFS measurements, and the error range in the curvature that originates from the non-perfect uniformity of the circle when making the bending (green horizontal markers). Making use of Eq. (3) and the known experimental conditions (θ_1 = 0 and θ_b = 0), the sensitivity α of the BFS on bending-

Optics EXPRESS

induced strain can be related to the slope S, as $\alpha = S/(\nu_B \cdot d_1)$. Using the values obtained from the measurements, and the known distance between Core 1 and the center of the fiber (d_1 is 39.252 ± 0.4062 μm), α is calculated to be equal to 4.88, being fairly identical to the well-known longitudinal strain coefficient of the BFS [5], thus supporting a solid consistency of the technique. It is also important to mention that errors in determining the BFS, d_1, and the slope S induce a negligible error in the determination of α. This can actually be evaluated by a simple calculation of the error propagation, considering that the errors in ν_B, d_1 and S are completely uncorrelated. This leads to an error (standard deviation) on α equal to 0.05, which represents a relative error of only 1%.

4.3. Demonstration of distributed shape sensing

Exploiting the calibrated curvature sensitivity, the setup in Fig. 2 has been used to demonstrate distributed shape sensing based on BOTDA in MCF. Different profiles have been patterned at the far end of the ~1 km long MCF. Figure 5 shows the profiles drawn for validation, including four U-like profiles and three O-like profiles, in which the bending radius (R_U and R_O) and arc length (L_U and L_O) have been marked in the figure for each profile. It should be noted that the cores orientation in the MCF has been positioned using the same visual procedure as previously described, and the bending angle along the whole interrogated fiber section has been carefully adjusted to be either 0 (or 2π) or π, with respect to the fiber core used as reference. Fixing this angle actually secures a better validation of the technique, since in this way curvatures and bending angles are known, providing a reference to compare with the measurements. Note that in Fig. 5 the fiber layout was prepared to illustrate clear representative situations spatially resolved by our distributed sensing system, since the path lengths of the O-like profiles are longer than the spatial resolution (20 cm) of the sensor, while the path lengths of the U-shapes are comparable to the spatial resolution of the system.

The BFS profiles measured along Core 1, Core 2 and Core 3 (see Fig. 1(b)) are presented in Fig. 6, where the U-shape and O-shape regions can be easily identified in Fig. 6(a) and 6(b), respectively.

Optics EXPRESS

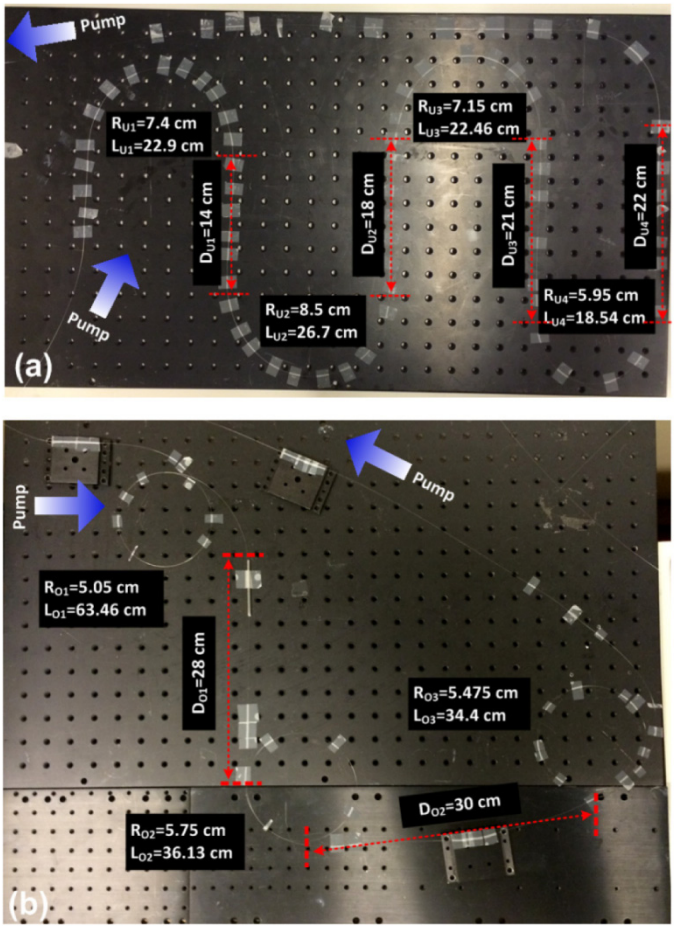

Fig. 5. Shapes made for validating the ability of distributed shape sensing based on BOTDA in MCF. (a) Four U-shapes, and (b) three O-shapes.

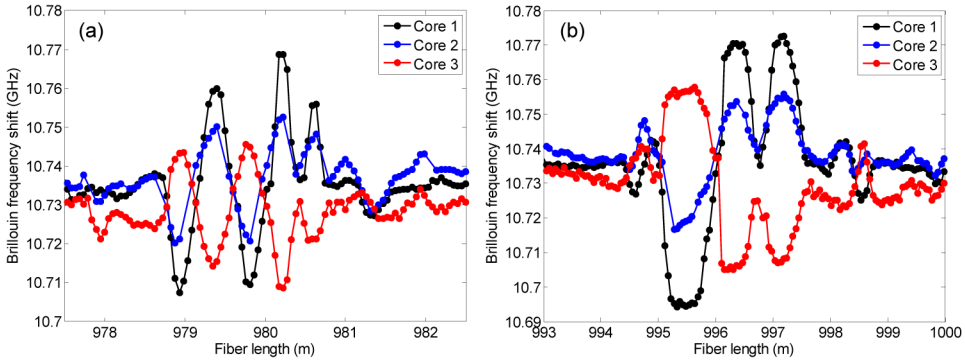

Fig. 6. BFS profiles versus distance, measured along three cores at (a) the 4 U-shape regions and (b) the 3 O-shape regions.

Calculations have been conducted by using the acquired BFS profiles in order to retrieve the bending angles and bending radius of the seven patterns. The measured variation of BFS has been first converted into strain using Eq. (3) with the sensitivity value $\alpha = 4.88$ obtained during characterization. The applied bending angle $\theta_b(z)$ and curvature $\kappa(z)$ of each pattern

Optics EXPRESS

are then obtained solving Eqs. (4)-(6). Figures 7(a) and 7(b) show the retrieved bending angles of the 4 U-profiles and 3 O-profiles, while Figs. 7(c) and 7(d) show the calculated curvature along the fiber. O-shapes have been labelled as "1" to "4" and U-shapes have been labelled as "5" to "7". An additional O-shape can be observed in Figs. 7(a) and 7(c), which corresponds to the quarter circle appearing on the upper right corner in Fig. 5(a); however this has not being labelled and further analyzed, since the actual length of this bent segment was shorter than the spatial resolution of the BOTDA system and its purpose was just to maintain the fiber on the plate.

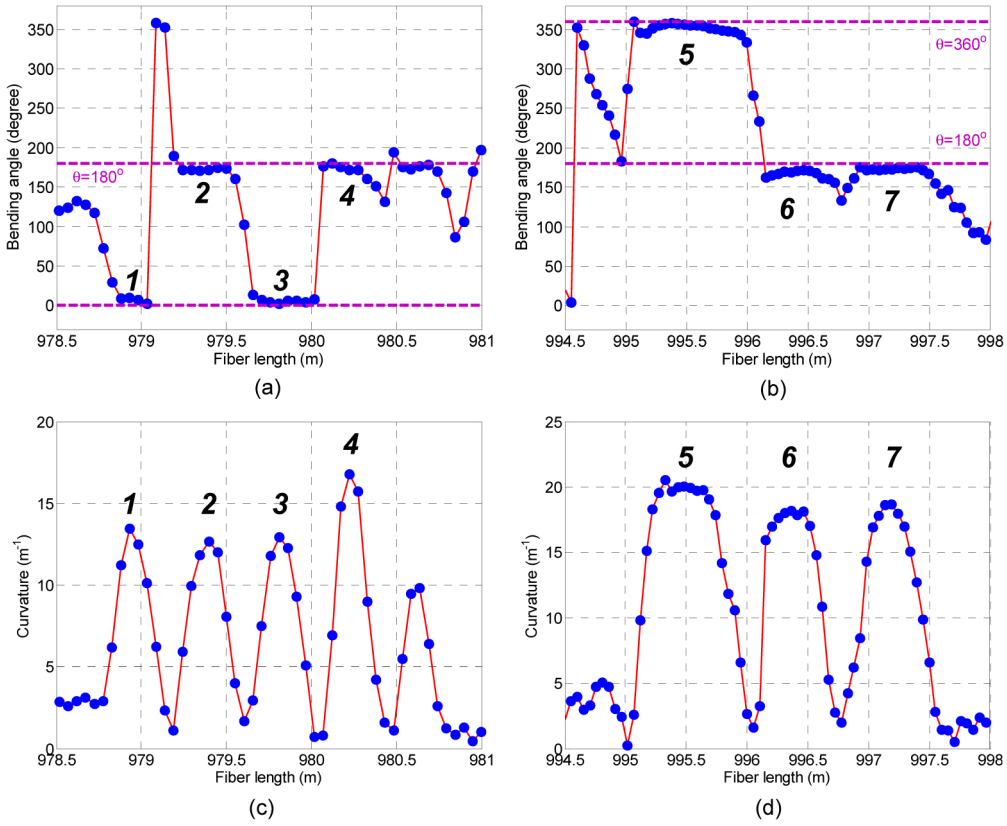

Fig. 7. Retrieved bending angle for (a) the 4 U-shape region; (b) the 3 O-shape region, and curvature for (c) the 4 U-shape region and (d) the 3 O-shape region. The blue dots represent the bending angle and curvature values obtained using Eqs. (4)-(6) and BFS measurements. Number "1" to "7" denotes the seven measured shapes.

Experimental results indicate that the retrieved bending angles and curvatures are all consistent with the calibrated position, where the bending plane is aligned to the local *x*-axis. This is consistent with the experimental conditions, in which the bending angle has been adjusted to 0 (or 2π) or π with respect to the chosen reference axis, as described previously. It should be however pointed out that the performed visual calibration procedure is by essence of limited precision, not better than 10 degrees, and fully explains the small differences between the expected and obtained values. The propagation of the error in the variables used to calculate the bending angle through Eqs. (4)-(5) has been evaluated. The result reveals that the uncertainty is in all cases very low, but increases at locations where the bending angle changes very fast. This is believed to be caused by the large levels of torsion and an eventually insufficient spatial resolution to measure fast torsion changes. However, within the fiber sections having a uniform bending angle, for example within the calibrated shape

Optics EXPRESS

regions, the standard deviation of the calculated bending angle and bending radius is very small (less than 2.22 degree and 0.28 cm, respectively). In particular the errors in the bending angle and bending radius for the 3 O-shapes are smaller than 1.5 degree and 0.15 cm, respectively. This better accuracy can be basically attributed to the longer bending lengths used for measuring the 3 O-shapes (much longer than the spatial resolution of 20 cm), while the length of the U-shapes is comparable to the spatial resolution, thus leading to slightly more inaccurate measurements.

The measurement mean value and relative root-mean-square (RMS) error on both the bending angle (θ_b) and the bending radius (R) are summarized in Table 1 for each of the seven measured shapes. The three first rows in the table show the parameters that have been set for the experiment, i.e. the length of each of the seven shapes as well as the mean values of the applied radius and bending angle. The error in the applied radius is in all cases below 0.15 cm, and in the bending angle below 10 degree. Then the mean value of the measured angles and radii, with their respective RMS errors, are shown from the fourth row in the table. Good matching is found between the measured and set values, leading to relative errors in the radius R below 8% in all cases.

Table 1. Applied and measured bending angle and radius for each patterned shape.

Shape	1st U	2nd U	3rd U	4th U	1st O	2nd O	3rd O
Length of the shape (cm)	22.90	26.70	22.46	18.54	63.46	36.13	34.40
Applied angle θ_B (degree)	0	180	0	180	0 (360)	180	180
Applied radius R (cm)	7.40	8.50	7.15	5.95	5.05	5.75	5.48
Measured angle θ_B (degree)	6.88	172.38	5.05	172.60	354.54	169.86	173.58
RMS error in angle (degre	2.20	2.14	2.22	1.63	1.41	1.50	1.48
Measured radius R (cm)	7.44	7.91	7.72	5.97	5.01	5.55	5.36
RMS error in radius (cm)	0.25	0.28	0.28	0.17	0.13	0.15	0.14
Relative error in radius (%	0.54	6.94	7.97	0.34	0.79	3.48	2.19

Note: The applied radius R is the bending radius of the patterned shapes, measured with an error below 0.15 cm; the applied angle has been carefully adjusted during calibration; however errors up to 10 degree are expected along the shapes. The measured angle and radius are the mean values obtained within each shape. Mean values and RMS errors are calculated using all longitudinal points inside the respective shape and considering 5 consecutive measurements.

Results demonstrate the high accuracy and good reliability of the method for distributed shape sensing. It must be however mentioned that better results can still be expected by improving the quality of the fan-in/out coupler used in the experiment. This is because the currently used fan-in/out coupler generates strong reflections, which give rise to an interference that overlaps with the relevant temporal trace, thus increasing the uncertainty on the BFS measurements.

5. Conclusion

A thorough experimental investigation on the impact of fiber bending on the response of Brillouin scattering in a multi-core fiber has been reported in this paper, for the first time to the best of our knowledge. Experimental and theoretical results have verified that the response to curvature of the Brillouin frequency of outer cores in a MCF shows great linearity, providing a straightforward technique to perform distributed curvature/bending sensing based on conventional Brillouin sensing schemes. Measuring the distributed profile of the curvature and bending angle along the fiber, as demonstrated in this paper, gives the basis to extend the technique to perform full 3D shape determination using an optical fiber in a distributed sensing configuration. For this purpose, the obtained curvature and bending angle

Optics EXPRESS

can be straightforwardly applied to solve a set of equations called Frenet-Serret formulas, as described in [15]. Compared to the 3D shape sensing techniques based on fiber Bragg gratings, the Brillouin scattering provides the possibility to perform distributed shape measurements continuously along a plain multi-core fiber, which does not require further processing as required for the generation of a Bragg grating. It must be mentioned that the BFS measurement along the different cores can be simultaneously performed by serially connecting the different cores in the same fiber and obtaining the response for all cores in a single trace. This could not be implemented in this study since the connection losses and the reflectivity were much too high in the fan-in/out spatial coupler, but can be straightforwardly realized using an improved device.

Funding

National 863 High-tech R&D Program of China (Grant No. 2013AA013402); National Natural Science Foundation of China (Grant No. 61331010, 61205063, 61290311); Program for New Century Excellent Talents in University (NCET-13-0235) of China; China Scholarship Council (NO. 201406160008)

Acknowledgments

The authors thank Dr. Huifeng Wei and Dr. Weijun Tong from Yangtze Optical Fiber and Cable Joint Stock Limited Company (YOFC) for providing the MCF, and EPFL-CIME for characterizing the geometry of the MCF. Z. Zhao acknowledges Dr. Andrey Denisov from EPFL-GFO for helpful discussion.